Engineering Analysis with Boundary Elements 34 (2010) 1064–1071

Contents lists available at ScienceDirect

Engineering Analysis with Boundary Elements

journal homepage: www.elsevier.com/locate/enganabound

Eigensolutions of a circular flexural plate with multiple circular holes by using the direct BIEM and addition theorem

W.M. Lee [a], J.T. Chen [b,c,*]

[a] Department of Mechanical Engineering, China University of Science and Technology, Taipei, Taiwan
[b] Department of Harbor and River Engineering, National Taiwan Ocean University, Keelung, Taiwan
[c] Department of Mechanical and Mechatronic Engineering, National Taiwan Ocean University, Keelung, Taiwan

ARTICLE INFO

Article history:
Received 26 November 2009
Accepted 26 June 2010
Available online 31 July 2010

Keywords:
Direct boundary integral equation
Null-field integral equation
Addition theorem
Complex Fourier series
Vibration
Spurious eigenvalue
SVD updating technique

ABSTRACT

The purpose of this paper is to present an analytical formulation to describe the free vibration of a circular flexural plate with multiple circular holes by using the null field integral formulation, the addition theorem and complex Fourier series. Owing to the addition theorem, all kernel functions are represented in the degenerate form and further transformed into the same polar coordinates centered at one of circles, where the boundary conditions are specified. Thus, not only the computation of the principal value for integrals is avoided but also the calculation of higher-order derivatives in the flexural plate problem can be easily determined. By matching the specified boundary conditions, a coupled infinite system of simultaneous linear algebraic equations is derived as an analytical model for the title problem. According to the direct searching approach, natural frequencies are numerically determined through the singular value decomposition (SVD) in the truncated finite system. After determining the unknown Fourier coefficients, the corresponding mode shapes are obtained by using the direct boundary integral formulations for the domain points. Several numerical results are presented. In addition, the inherent problem of spurious eigenvalue using the integral formulation is investigated and the SVD updating technique is adopted to suppress the occurrence of spurious eigenvalues. Excellent accuracy, fast rate of convergence and high computational efficiency are advantages of the present method thanks to its analytical features.

1. Introduction

Circular plates with multiple circular holes are widely used in engineering structures [1], e.g. missiles, aircraft, etc., either to reduce the weight of the structure, to increase the range of inspection or to satisfy other engineering applications. These holes in a structure usually invoke natural frequency change and loading capacity decrease. It is important to comprehend the corresponding effects in the process of mechanical design.

As quoted by Leissa and Narita [2]: "The free vibrations of circular plates have been of practical and academic interest for at least a century and a half", over the past few decades, most of the researches have focused on the analytical solutions for natural frequencies of the circular or annular plates [3–6]. Recently some researchers tried to extend the analysis of an annular plate [7,8] to that of a plate with an eccentric circular hole. Laura et al. [8] determined the natural frequencies of circular plate with an eccentric circular hole by using the Rayleigh–Ritz variational method where the assumed function does not satisfy the natural boundary condition in the inner free edge. Lee and Chen [9,10] proposed a semi-analytical approach to solve the free vibration analysis of a circular plate with multiple holes by using the indirect boundary integral method and the null field boundary integral equation method (BIEM) and pointed out certain insufficient accurate results in [8] after careful comparisons.

It is clear that unknowns of problem can be dramatically reduced by using boundary element method (BEM) or BIEM in comparison to the traditional domain type methods such as FDM or FEM. For applications of the BEM on plate problems, readers may consult with the review article [11]. By using the BIEM to analytically solve the problem of a circular plate with multiple circular holes, two questions need to be solved. One is the improper integral in the boundary integral equation; the other is that both field point and source point are not located on the same circular boundary. These problems have been treated by using the degenerate kernel and tensor transformation [9,10], respectively. However, tensor transformation accompanied by higher order derivatives, such as those in effective shear force, tends to increase the complexity of computation and then affect the accuracy of its solution [9]. In addition, the collocation method in [9,10] belongs to a point-matching approach instead of an

* Corresponding author.
E-mail addresses: wmlee@cc.cust.edu.tw (W.M. Lee), jtchen@mail.ntou.edu.tw (J.T. Chen).

0955-7997/$ - see front matter © 2010 Elsevier Ltd. All rights reserved.
doi:10.1016/j.enganabound.2010.06.018

analytical derivation. It also increases the effort of computation since boundary nodes for collocation are required.

This paper presents an analytical methodology to solve the free vibration problem of a multiply-connected domain plate free of collocation points and the tensor transformation. When considering a circular plate with multiple circular holes in the direct boundary integral formulation, the transverse displacement field is represented by all local coordinates centered at each center of circles. By using the addition theorem, it can be transformed into the same coordinate centered at one of circles, where the boundary conditions are specified. By this way, the higher derivative such as bending moments and effective shear forces can be easily determined due to one variable involved. According to the specified boundary conditions, a coupled infinite system of simultaneous linear algebraic equations is obtained. In the finite truncated system, the direct searching approach [12] is adopted to determine the natural frequency through the singular value decomposition (SVD) technique [13] by finding the zero determinant of the matrix. After determining the unknown Fourier coefficients, the corresponding mode shapes are obtained by using the direct boundary integral equation for domain points. The convergence analysis is performed on the terms of the complex Fourier series. The proposed results of a circular plate with three circular holes are compared with those of the semi-analytical method [10] and of the FEM using the ABAQUS [14]. Moreover, the inherent problem of spurious eigenvalue using the BEM is investigated and the SVD updating technique [10] is employed to suppress the appearance of spurious eigenvalues.

2. Problem statement and a direct boundary integral formulation

2.1. Problem statement of a plate eigenproblem

A uniform thin circular plate with H nonoverlapping circular holes centered at the position vector O_k (k=0, 1,…,H; O_0 is the position vector of the outer circular boundary of the plate) has a domain Ω which is enclosed with boundary,

$$B = \bigcup_{k=0}^{H} B_k \tag{1}$$

as shown in Fig. 1, where R_k denotes the radius of the kth circle and B_k is its corresponding boundary. The governing equation of the free vibration for this flexural plate is expressed as

$$\nabla^4 u(\boldsymbol{x}) = \lambda^4 u(\boldsymbol{x}), \quad \boldsymbol{x} \in \Omega \tag{2}$$

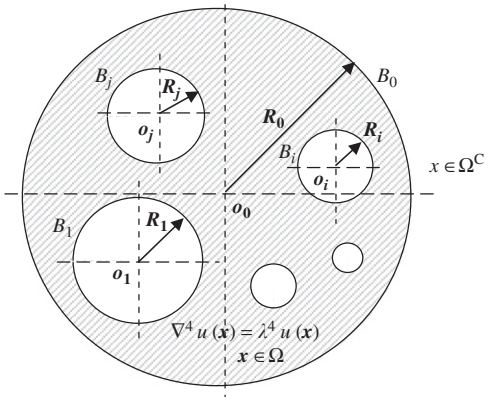

Fig. 1. Problem statement for an eigenproblem of a circular plate with multiple circular holes.

where ∇^4 is the biharmonic operator, u is the lateral displacement, $\lambda^4 = \omega^2 \rho_0 h/D$, λ is the dimensionless frequency parameter, ω is the circular frequency, ρ_0 is the volume density, h is the plate thickness, $D = Eh^3/12(1-\mu^2)$ is the flexural rigidity of the plate, E denotes the Young's modulus and μ is the Poisson's ratio.

2.2. Direct boundary integral formulation

The integral representation for the plate problem can be derived from the Rayleigh–Green identity [12] as follows:

$$u(\boldsymbol{x}) = \int_B U(\boldsymbol{s},\boldsymbol{x}) v(\boldsymbol{s})\, dB(\boldsymbol{s}) - \int_B \Theta(\boldsymbol{s},\boldsymbol{x}) m(\boldsymbol{s})\, dB(\boldsymbol{s}) + \int_B M(\boldsymbol{s},\boldsymbol{x}) \theta(\boldsymbol{s})\, dB(\boldsymbol{s}) - \int_B V(\boldsymbol{s},\boldsymbol{x}) u(\boldsymbol{s})\, dB(\boldsymbol{s}), \quad \boldsymbol{x} \in \Omega \tag{3}$$

$$\theta(\boldsymbol{x}) = \int_B U_\theta(\boldsymbol{s},\boldsymbol{x}) v(\boldsymbol{s})\, dB(\boldsymbol{s}) - \int_B \Theta_\theta(\boldsymbol{s},\boldsymbol{x}) m(\boldsymbol{s})\, dB(\boldsymbol{s}) + \int_B M_\theta(\boldsymbol{s},\boldsymbol{x}) \theta(\boldsymbol{s})\, dB(\boldsymbol{s}) - \int_B V_\theta(\boldsymbol{s},\boldsymbol{x}) u(\boldsymbol{s})\, dB(\boldsymbol{s}), \quad \boldsymbol{x} \in \Omega \tag{4}$$

$$m(\boldsymbol{x}) = \int_B U_m(\boldsymbol{s},\boldsymbol{x}) v(\boldsymbol{s})\, dB(\boldsymbol{s}) - \int_B \Theta_m(\boldsymbol{s},\boldsymbol{x}) m(\boldsymbol{s})\, dB(\boldsymbol{s}) + \int_B M_m(\boldsymbol{s},\boldsymbol{x}) \theta(\boldsymbol{s})\, dB(\boldsymbol{s}) - \int_B V_m(\boldsymbol{s},\boldsymbol{x}) u(\boldsymbol{s})\, dB(\boldsymbol{s}), \quad \boldsymbol{x} \in \Omega \tag{5}$$

$$v(\boldsymbol{x}) = \int_B U_v(\boldsymbol{s},\boldsymbol{x}) v(\boldsymbol{s})\, dB(\boldsymbol{s}) - \int_B \Theta_v(\boldsymbol{s},\boldsymbol{x}) m(\boldsymbol{s})\, dB(\boldsymbol{s}) + \int_B M_v(\boldsymbol{s},\boldsymbol{x}) \theta(\boldsymbol{s})\, dB(\boldsymbol{s}) - \int_B V_v(\boldsymbol{s},\boldsymbol{x}) u(\boldsymbol{s})\, dB(\boldsymbol{s}), \quad \boldsymbol{x} \in \Omega \tag{6}$$

where B is the boundary of the domain Ω, $u(\boldsymbol{x})$, $\theta(\boldsymbol{x})$, $m(\boldsymbol{x})$ and $v(\boldsymbol{x})$ are the displacement, slope, moment and shear force. The notations $\boldsymbol{s}$ and $\boldsymbol{x}$ mean the source and field points, respectively. The kernel functions $U(\boldsymbol{s},\boldsymbol{x})$, $\Theta(\boldsymbol{s},\boldsymbol{x})$, $M(\boldsymbol{s},\boldsymbol{x})$, $V(\boldsymbol{s},\boldsymbol{x})$, $U_\theta(\boldsymbol{s},\boldsymbol{x})$, $\Theta_\theta(\boldsymbol{s},\boldsymbol{x})$, $M_\theta(\boldsymbol{s},\boldsymbol{x})$,$V_\theta(\boldsymbol{s},\boldsymbol{x})$, $U_m(\boldsymbol{s},\boldsymbol{x})$, $\Theta_m(\boldsymbol{s},\boldsymbol{x})$, $M_m(\boldsymbol{s},\boldsymbol{x})$, $V_m(\boldsymbol{s},\boldsymbol{x})$, $U_v(\boldsymbol{s},\boldsymbol{x})$, $\Theta_v(\boldsymbol{s},\boldsymbol{x})$, $M_v(\boldsymbol{s},\boldsymbol{x})$ and $V_v(\boldsymbol{s},\boldsymbol{x})$ in Eqs. (3)–(6) can be expanded to degenerate kernels by separating the source and field points and will be elaborated on later. The kernel function $U(\boldsymbol{s},\boldsymbol{x})$ in Eq. (3):

$$U(\boldsymbol{s},\boldsymbol{x}) = \frac{1}{8\lambda^2 D}\left[Y_0(\lambda r) - iJ_0(\lambda r) + \frac{2}{\pi} K_0(\lambda r)\right] \tag{7}$$

is the fundamental solution which satisfies

$$\nabla^4 U(\boldsymbol{s},\boldsymbol{x}) - \lambda^4 U(\boldsymbol{s},\boldsymbol{x}) = \delta(\boldsymbol{s}-\boldsymbol{x}) \tag{8}$$

where $\delta(\boldsymbol{s}-\boldsymbol{x})$ is the Dirac-delta function, $Y_0(\lambda r)$ and $K_0(\lambda r)$ are the zeroth-order of the second-kind Bessel and modified Bessel functions, respectively, $J_0(\lambda r)$ is the zeroth-order of the first-kind Bessel function, $r \equiv |\boldsymbol{s}-\boldsymbol{x}|$ and $i^2 = -1$. The other three kernel functions, $\Theta(\boldsymbol{s},\boldsymbol{x})$, $M(\boldsymbol{s},\boldsymbol{x})$ *and* $V(\boldsymbol{s},\boldsymbol{x})$ in Eq. (3) can be obtained by applying the following slope, moment and effective shear operators defined by

$$K_\Theta = \frac{\partial(\cdot)}{\partial n} \tag{9}$$

$$K_M = -D\left[\mu\nabla^2(\cdot) + (1-\mu)\frac{\partial^2(\cdot)}{\partial n^2}\right] \tag{10}$$

$$K_V = -D\left[\frac{\partial}{\partial n}\nabla^2(\cdot) + (1-\mu)\frac{\partial}{\partial t}\left(\frac{\partial}{\partial n}\left(\frac{\partial}{\partial t}(\cdot)\right)\right)\right] \tag{11}$$

to the kernel $U(\boldsymbol{s},\boldsymbol{x})$ with respect to the source point, where $\partial/\partial n$ and $\partial/\partial t$ are the normal and tangential derivatives, respectively, ∇^2 means the Laplacian operator.

2.3. Null-field integral equations

The null-field integral equations can be derived from boundary integral equations of Eqs. (3)–(6) and by moving the field point outside the domain (including the boundary point if exterior degenerate kernels are properly adopted). They are explicitly expressed as follows:

$$0=\int_B U(\boldsymbol{s},\boldsymbol{x})v(\boldsymbol{s})\,dB(\boldsymbol{s})-\int_B \Theta(\boldsymbol{s},\boldsymbol{x})m(\boldsymbol{s})\,dB(\boldsymbol{s}) +\int_B M(\boldsymbol{s},\boldsymbol{x})\theta(\boldsymbol{s})\,dB(\boldsymbol{s})-\int_B V(\boldsymbol{s},\boldsymbol{x})u(\boldsymbol{s})\,dB(\boldsymbol{s}),\quad \boldsymbol{x}\in\Omega^C\cup B \tag{12}$$

$$0=\int_B U_\theta(\boldsymbol{s},\boldsymbol{x})v(\boldsymbol{s})\,dB(\boldsymbol{s})-\int_B \Theta_\theta(\boldsymbol{s},\boldsymbol{x})m(\boldsymbol{s})\,dB(\boldsymbol{s}) +\int_B M_\theta(\boldsymbol{s},\boldsymbol{x})\theta(\boldsymbol{s})\,dB(\boldsymbol{s})-\int_B V_\theta(\boldsymbol{s},\boldsymbol{x})u(\boldsymbol{s})\,dB(\boldsymbol{s}),\quad \boldsymbol{x}\in\Omega^C\cup B \tag{13}$$

$$0=\int_B U_m(\boldsymbol{s},\boldsymbol{x})v(\boldsymbol{s})\,dB(\boldsymbol{s})-\int_B \Theta_m(\boldsymbol{s},\boldsymbol{x})m(\boldsymbol{s})\,dB(\boldsymbol{s}) +\int_B M_m(\boldsymbol{s},\boldsymbol{x})\theta(\boldsymbol{s})\,dB(\boldsymbol{s})-\int_B V_m(\boldsymbol{s},\boldsymbol{x})u(\boldsymbol{s})\,dB(\boldsymbol{s}),\quad \boldsymbol{x}\in\Omega^C\cup B \tag{14}$$

$$0=\int_B U_v(\boldsymbol{s},\boldsymbol{x})v(\boldsymbol{s})\,dB(\boldsymbol{s})-\int_B \Theta_v(\boldsymbol{s},\boldsymbol{x})m(\boldsymbol{s})\,dB(\boldsymbol{s}) +\int_B M_v(\boldsymbol{s},\boldsymbol{x})\theta(\boldsymbol{s})\,dB(\boldsymbol{s})-\int_B V_v(\boldsymbol{s},\boldsymbol{x})u(\boldsymbol{s})\,dB(\boldsymbol{s}),\quad \boldsymbol{x}\in\Omega^C\cup B \tag{15}$$

where Ω^C is the complementary domain of Ω. It is noted that once kernel functions are expressed in proper degenerate forms, which will be elaborated in the next subsection, the field points can be exactly located on the real boundary, that is $\boldsymbol{x}\in\Omega^C\cup B$. Since the four equations of Eqs. (12)–(15) in the plate formulation are provided, there are 6 (C_2^4) options for choosing any two equations to solve the problem. To simply treat spurious eigenvalues, Eqs. (12)–(14) are all employed to solve this plate problem.

2.4. Degenerate kernels and Fourier series for boundary densities

In the polar coordinates, the field point and source point can be expressed as (ρ,ϕ) and (R,θ), respectively. By employing the addition theorem [15], the kernel function $U(\boldsymbol{s},\boldsymbol{x})$is expanded in the series form as follows:

$$U:\begin{cases} U^I(\boldsymbol{s},\boldsymbol{x})=\dfrac{1}{8\lambda^2 D}\displaystyle\sum_{m=-\infty}^{\infty}\{J_m(\lambda\rho)[Y_m(\lambda R)-iJ_m(\lambda R)]+\frac{2}{\pi}I_m(\lambda\rho)K_m(\lambda R)\}e^{im(\phi-\theta)}, & \rho<R,\\ U^E(\boldsymbol{s},\boldsymbol{x})=\dfrac{1}{8\lambda^2 D}\displaystyle\sum_{m=-\infty}^{\infty}\{J_m(\lambda R)[Y_m(\lambda\rho)-iJ_m(\lambda\rho)]+\frac{2}{\pi}I_m(\lambda R)K_m(\lambda\rho)\}e^{im(\phi-\theta)}, & \rho\ge R,\end{cases} \tag{16}$$

where the superscripts "I" and "E" denote the interior and exterior cases for $U(\boldsymbol{s},\boldsymbol{x})$ degenerate kernel to distinguish $\rho<R$ and $\rho>R$, respectively, as shown in Fig. 2. The degenerate kernels of $\Theta(\boldsymbol{s},\boldsymbol{x})$, $M(\boldsymbol{s},\boldsymbol{x})$ and $V(\boldsymbol{s},\boldsymbol{x})$ in the null-field boundary integral equations can be obtained by applying the operators of Eqs. (9)–(11) to the degenerate kernel $U(\boldsymbol{s},\boldsymbol{x})$ in Eq. (16) with respect to the source point $\boldsymbol{s}$.

In order to fully utilize the geometry of circular boundary and to solve the multiply-connected problem, the displacement $u(\boldsymbol{s})$, slope $\theta(\boldsymbol{s})$, moment $m(\boldsymbol{s})$ and shear force $v(\boldsymbol{s})$ along the circular boundaries in the null-field integral equations can be expanded in terms of complex Fourier series, respectively, as follows:

$$u^k(\boldsymbol{s_k})=\sum_{n=-\infty}^{\infty}a_n^k e^{in\theta_k},\quad \boldsymbol{s_k}\in B_k,\quad k=0,\ldots,H \tag{17}$$

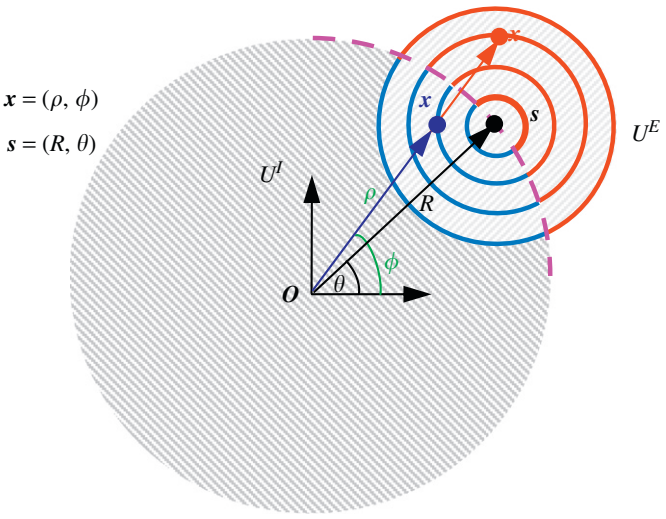

Fig. 2. Degenerate kernel for $U(\boldsymbol{s},\boldsymbol{x})$.

$$\theta^k(\boldsymbol{s_k})=\sum_{n=-\infty}^{\infty}b_n^k e^{in\theta_k},\quad \boldsymbol{s_k}\in B_k,\quad k=0,\ldots,H \tag{18}$$

$$m^k(\boldsymbol{s_k})=\sum_{n=-\infty}^{\infty}c_n^k e^{in\theta_k},\quad \boldsymbol{s_k}\in B_k,\quad k=0,\ldots,H \tag{19}$$

$$v^k(\boldsymbol{s_k})=\sum_{n=-\infty}^{\infty}d_n^k e^{in\theta_k},\quad \boldsymbol{s_k}\in B_k,\quad k=0,\ldots,H \tag{20}$$

where a_n^k, b_n^k, $c_n^k$and d_n^k are the complex Fourier coefficients of the kth circular boundary and θ_k is its polar angle, H is the number of inner holes.

3. An analytical eigensolution for a circular plate with multiple circular holes

For simplicity, a clamped circular plate ($u^0=\theta^0=0$) with H circular holes subject to the free-traction boundary conditions ($m^k=v^k=0$, $k=1,\ldots,H$) is demonstrated. Considering the null field point near the circular boundary B_0 and the geometrical relation between this point and each circular boundary, substitution of the proper degenerated kernel functions into Eq. (12) gives

$$0=\int_{B_0}U^E(\boldsymbol{s}_0,\boldsymbol{x}_0)v^0(\boldsymbol{s}_0)dB_0(\boldsymbol{s}_0)-\int_{B_0}\Theta^E(\boldsymbol{s}_0,\boldsymbol{x}_0)m^0(\boldsymbol{s}_0)\,dB_0(\boldsymbol{s}_0) -\left[\sum_{k=1}^{H}\int_{B_k}M^E(\boldsymbol{s}_k,\boldsymbol{x}_k)\theta^k(\boldsymbol{s}_k)\,dB_k(\boldsymbol{s}_k)-\int_{B_k}V^E(\boldsymbol{s}_k,\boldsymbol{x}_k)u^k(\boldsymbol{s}_k)\,dB_k(\boldsymbol{s}_k)\right] \tag{21}$$

By substituting the degenerate kernels, such as Eq. (16), and the boundary densities of Eqs. (17)–(20) into Eq. (21) in the adaptive coordinate system [10], we have

$$0=\int_{B_0}\left(\frac{1}{8\lambda^2 D}\sum_{m=-\infty}^{\infty}\{J_m(\lambda R_0)[Y_m(\lambda\rho_0)-iJ_m(\lambda\rho_0)],\right.$$

$$+\frac{2}{\pi}I_m(\lambda R_0)K_m(\lambda\rho_0)\Big\}e^{im(\phi_0-\theta_0)}\Big)\left(\sum_{n=-\infty}^{\infty}d_n^0e^{in\theta_0}\right)dB_0(s_0)$$
$$-\int_{B_0}\left(\frac{1}{8\lambda D}\sum_{m=-\infty}^{\infty}\Big\{J'_m(\lambda R_0)[Y_m(\lambda\rho_0)-iJ_m(\lambda\rho_0]$$
$$+\frac{2}{\pi}I'_m(\lambda R_0)K_m(\lambda\rho_0)\Big\}e^{im(\phi_0-\theta_0)}\Big)\left(\sum_{n=-\infty}^{\infty}c_n^0e^{in\theta_0}\right)dB_0(s_0)$$
$$-\sum_{k=1}^{H}\Bigg[-\int_{B_k}\left(\frac{1}{8\lambda^2}\sum_{m=-\infty}^{\infty}\Big\{J_m(\lambda\rho_k)[\alpha_m^Y(\lambda R_k)-i\alpha_m^J(\lambda R_k)]$$
$$+\frac{2}{\pi}I_m(\lambda\rho_k)\alpha_m^K(\lambda R_k)\Big\}e^{im(\phi_k-\theta_k)}\Big)\left(\sum_{n=-\infty}^{\infty}b_n^ke^{in\theta_k}\right)dB_k(s_k)$$
$$+\int_{B_k}\left(\frac{1}{8\lambda^2}\sum_{m=-\infty}^{\infty}\Big\{J_m(\lambda\rho_k)[\beta_m^Y(\lambda R_k)-i\beta_m^J(\lambda R_k)]$$
$$+\frac{2}{\pi}I_m(\lambda\rho_k)\beta_m^K(\lambda R_k)\Big\},e^{im(\phi_k-\theta_k)}\Big)\left(\sum_{n=-\infty}^{\infty}a_n^ke^{in\theta_k}\right)dB_k(s_k)\Bigg] \tag{22}$$

where the (ρ_0,ϕ_0), $(\rho_1,\phi),\ldots,(\rho_H,\phi_H)$ are the coordinates for the field point $\boldsymbol{x}$ with respect to each center of circles. From Eqs. (10) and (11), the moment and the effective shear operators, $\alpha_m^X(\lambda\rho)$ and $\beta_m^X(\lambda\rho)$ are defined by, respectively,

$$\alpha_m^X(\lambda\rho)=D\left\{(1-\mu)\frac{X'_m(\lambda\rho)}{\rho}-\left[(1-\mu)\frac{m^2}{\rho^2}\mp\lambda^2\right]X_m(\lambda\rho)\right\} \tag{23}$$

$$\beta_m^X(\lambda\rho)=D\left\{\left[m^2(1-\mu)\pm(\lambda\rho)^2\right]\frac{X'_m(\lambda\rho)}{\rho^2}-m^2(1-\mu)\frac{X_m(\lambda\rho)}{\rho^3}\right\} \tag{24}$$

where the upper (lower) signs refer to $X=J$, Y, (I, K), respectively. The second order differential equations for these functions have been used to simplify $\alpha_m^X(\lambda\rho)$ and $\beta_m^X(\lambda\rho)$.

By employing the analytical integration along each circular boundary in the local coordinate and applying the orthogonal property, Eq. (22) can be rewritten as

$$0=\frac{\pi R_0}{4\lambda^2D}\sum_{m=-\infty}^{\infty}\Big\{J_m(\lambda R_0)[Y_m(\lambda\rho_0)-iJ_m(\lambda\rho_0)]$$
$$+\frac{2}{\pi}I_m(\lambda R_0)K_m(\lambda\rho_0)\Big\}d_m^0e^{im\phi_0}$$
$$-\frac{\pi R_0}{4\lambda D}\sum_{m=-\infty}^{\infty}\Big\{J'_m(\lambda R_0)[Y_m(\lambda\rho_0)-iJ_m(\lambda\rho_0)]$$
$$+\frac{2}{\pi}I'_m(\lambda R_0)K_m(\lambda\rho_0)\Big\}c_m^0e^{im\phi_0}$$
$$-\sum_{k=1}^{H}\Bigg[-\frac{\pi R_k}{4\lambda^2}\sum_{m=-\infty}^{\infty}\Big\{J_m(\lambda\rho_k)[\alpha_m^Y(\lambda R_k)-i\alpha_m^J(\lambda R_k)]$$
$$+\frac{2}{\pi}I_m(\lambda\rho_k)\alpha_m^K(\lambda R_k)\Big\}b_m^ke^{im\phi_k}$$
$$+\frac{\pi R_k}{4\lambda^2}\sum_{m=-\infty}^{\infty}\Big\{J_m(\lambda\rho_k)[\beta_m^Y(\lambda R_k)-i\beta_m^J(\lambda R_k)]$$
$$+\frac{2}{\pi}I_m(\lambda\rho_k)\beta_m^K(\lambda R_k)\Big\}a_m^ke^{im\phi_k}\Bigg] \tag{25}$$

Based on Graf's addition theorem for Bessel functions given in [15,16], we can express the theorem in the following form:

$$J_m(\lambda\rho_k)e^{im\phi_k}=\sum_{n=-\infty}^{\infty}J_{m-n}(\lambda r_{kp})e^{i(m-n)\theta_{kp}}J_n(\lambda\rho_p)e^{in\phi_p} \tag{26}$$

$$I_m(\lambda\rho_k)e^{im\phi_k}=\sum_{n=-\infty}^{\infty}I_{m-n}(\lambda r_{kp})e^{i(m-n)\theta_{kp}}I_n(\lambda\rho_p)e^{in\phi_p} \tag{27}$$

$$Y_m(\lambda\rho_k)e^{im\phi_k}=\begin{cases}\displaystyle\sum_{n=-\infty}^{\infty}Y_{m-n}(\lambda r_{kp})e^{i(m-n)\theta_{kp}}J_n(\lambda\rho_p)e^{in\phi_p}, & \rho_p<r_{kp}\\ \displaystyle\sum_{n=-\infty}^{\infty}J_{m-n}(\lambda r_{kp})e^{i(m-n)\theta_{kp}}Y_n(\lambda\rho_p)e^{in\phi_p}, & \rho_p>r_{kp}\end{cases} \tag{28}$$

$$K_m(\lambda\rho_k)e^{im\phi_k}=\begin{cases}\displaystyle\sum_{n=-\infty}^{\infty}(-1)^nK_{m-n}(\lambda r_{kp})e^{i(m-n)\theta_{kp}}I_n(\lambda\rho_p)e^{in\phi_p}, & \rho_p<r_{kp}\\ \displaystyle\sum_{n=-\infty}^{\infty}(-1)^{m-n}I_{m-n}(\lambda r_{kp})e^{i(m-n)\theta_{kp}}K_n(\lambda\rho_p)e^{in\phi_p}, & \rho_p>r_{kp}\end{cases} \tag{29}$$

where (ρ_p,ϕ_p) and (ρ_k,ϕ_k) as shown in Fig. 3 are the polar coordinates of a typical field point $\boldsymbol{x}$ with respect to O_p and O_k, respectively, which are the origins of two polar coordinate systems and (r_{kp},θ_{kp}) are the polar coordinates of O_p with respect to O_k.

By using the addition theorem for Bessel functions $J_m(\lambda\rho_k)$, $Y_m(\lambda\rho_k)$ and $K_m(\lambda\rho_k)$, under the condition of $\rho_0>r_{k0}$, Eq. (25) can be expanded as follows:

$$0=\frac{\pi R_0}{4\lambda^2D}\sum_{m=-\infty}^{\infty}\Big\{J_m(\lambda R_0)[Y_m(\lambda\rho_0)-iJ_m(\lambda\rho_0)]+\frac{2}{\pi}I_m(\lambda R_0)K_m(\lambda\rho_0)\Big\}d_m^0e^{im\phi_0}$$
$$-\frac{\pi R_0}{4\lambda D}\sum_{m=-\infty}^{\infty}\Big\{J'_m(\lambda R_0)[Y_m(\lambda\rho_0)-iJ_m(\lambda\rho_0)]+\frac{2}{\pi}I'_m(\lambda R_0)K_m(\lambda\rho_0)\Big\}c_m^0e^{im\phi_0}$$
$$+\sum_{k=1}^{H}\Bigg[\frac{\pi R_k}{4\lambda^2}\sum_{m=-\infty}^{\infty}\Big\{[\alpha_m^Y(\lambda R_k)-i\alpha_m^J(\lambda R_k)]\sum_{n=-\infty}^{\infty}J_{m-n}(\lambda r_{k0})e^{i(m-n)\theta_{k0}}J_n(\lambda\rho_0)$$
$$+\frac{2}{\pi}\alpha_m^K(\lambda R_k)\sum_{n=-\infty}^{\infty}I_{m-n}(\lambda r_{k0})e^{i(m-n)\theta_{k0}}I_n(\lambda\rho_0)\Big\}e^{in\phi_0}b_m^k$$
$$-\frac{\pi R_k}{4\lambda^2}\sum_{m=-\infty}^{\infty}\Big\{[\beta_m^Y(\lambda R_k)-i\beta_m^J(\lambda R_k)]\sum_{n=-\infty}^{\infty}J_{m-n}(\lambda r_{k0})e^{i(m-n)\theta_{k0}}J_n(\lambda\rho_0)$$
$$+\frac{2}{\pi}\beta_m^K(\lambda R_k)\sum_{n=-\infty}^{\infty}I_{m-n}(\lambda r_{k0})e^{i(m-n)\theta_{k0}}I_n(\lambda\rho_0)\Big\}e^{in\phi_0}a_m^k\Bigg] \tag{30}$$

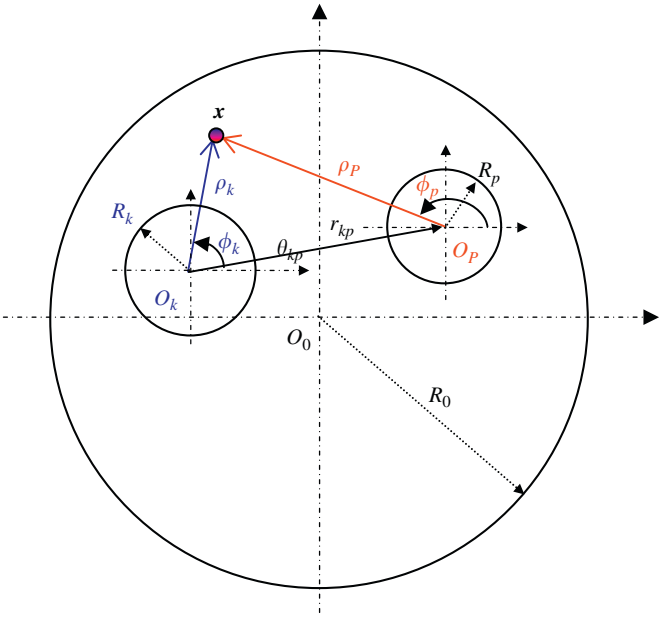

Fig. 3. Notation of the Graf's addition theorem for Bessel functions.

Furthermore, Eq. (30) can be rewritten as

$$0=\sum_{m=-\infty}^{\infty}e^{im\phi_0}\left\langle A_m^0(\lambda\rho_0)d_m^0+B_m^0(\lambda\rho_0)c_m^0 +\sum_{k=1}^{H}\left[\sum_{n=-\infty}^{\infty}A_{mn}^k(\lambda\rho_0)b_n^k+\sum_{n=-\infty}^{\infty}B_{mn}^k(\lambda\rho_0)a_n^k\right]\right\rangle \tag{31}$$

where

$$A_m^0(\lambda\rho_0)=\frac{\pi R_0}{4\lambda^2 D}\left\{J_m(\lambda R_0)[Y_m(\lambda\rho_0)-iJ_m(\lambda\rho_0)]+\frac{2}{\pi}I_m(\lambda R_0)K_m(\lambda\rho_0)\right\} \tag{32}$$

$$B_m^0(\lambda\rho_0)=-\frac{\pi R_0}{4\lambda D}\left\{J'_m(\lambda R_0)[Y_m(\lambda\rho_0)-iJ_m(\lambda\rho_0)]+\frac{2}{\pi}I'_m(\lambda R_0)K_m(\lambda\rho_0)\right\} \tag{33}$$

$$A_{mn}^k(\lambda\rho_0)=\frac{\pi R_k}{4\lambda^2}e^{i(n-m)\theta_{k0}}\left\{J_{n-m}(\lambda r_{k0})\alpha_n^J(\lambda R_k)[Y_m(\lambda\rho_0)-iJ_m(\lambda\rho_0)] +\frac{2}{\pi}(-1)^{n-m}I_{n-m}(\lambda r_{k0})\alpha_n^J(\lambda R_k)K_m(\lambda\rho_0)\right\} \tag{34}$$

$$B_{mn}^k(\lambda\rho_0)=-\frac{\pi R_k}{4\lambda^2}e^{i(n-m)\theta_{k0}}\left\{J_{n-m}(\lambda r_{k0})\beta_n^J(\lambda R_k)[Y_m(\lambda\rho_0)-iJ_m(\lambda\rho_0)] +\frac{2}{\pi}(-1)^{n-m}I_{n-m}(\lambda r_{k0})\beta_n^I(\lambda R_k)K_m(\lambda\rho_0)\right\} \tag{35}$$

By differentiating Eq. (31) with respect to ρ_0, the equation for the slope θ near the circular boundary B_0 is given as

$$0=\sum_{m=-\infty}^{\infty}e^{im\phi_0}\left\langle C_m^0(\lambda\rho_0)d_m^0+D_m^0(\lambda\rho_0)c_m^0 +\sum_{k=1}^{H}\left[\sum_{n=-\infty}^{\infty}C_{mn}^k(\lambda\rho_0)b_n^k+\sum_{n=-\infty}^{\infty}D_{mn}^k(\lambda\rho_0)a_n^k\right]\right\rangle \tag{36}$$

where $C_m^0(\lambda\rho_0)$, $D_m^0(\lambda\rho_0)$, $C_{mn}^k(\lambda\rho_0)$ and $D_{mn}^k(\lambda\rho_0)$ can be obtained by differentiating $A_m^0(\lambda\rho_0)$, $B_m^0(\lambda\rho_0)$, $A_{mn}^k(\lambda\rho_0)$ and $B_{mn}^k(\lambda\rho_0)$ in Eqs. (32)–(35) with respective to ρ_0.

Similarly, considering the null field point near the circular boundary B_p ($p=1,\ldots,H$) and the geometrical relation between this point and each circular boundary, substitution of the proper degenerated kernel functions into Eq. (12) gives

$$0=\int_{B_0}U^I(\boldsymbol{s}_0,\boldsymbol{x}_0)v^0(\boldsymbol{s}_0)dB_0(\boldsymbol{s}_0)-\int_{B_0}\Theta^I(\boldsymbol{s}_0,\boldsymbol{x}_0)m^0(\boldsymbol{s}_0)dB_0(\boldsymbol{s}_0) -\left[\sum_{k=1}^{H}\int_{B_k}M^q(\boldsymbol{s}_k,\boldsymbol{x}_k)\theta^k(\boldsymbol{s}_k)dB_k(\boldsymbol{s}_k)-\int_{B_k}V^q(\boldsymbol{s}_k,\boldsymbol{x}_k)u^k(\boldsymbol{s}_k)dB_k(\boldsymbol{s}_k)\right] \tag{37}$$

where $q=I$, $p=k$; $q=E$, $p\neq k$.

By substituting the proper degenerate kernel functions and the complex Fourier series into Eq. (37), employing the analytical integration along each circular boundary, applying the orthogonal property and then using the addition theorem, Eq. (37) yields

$$0=\sum_{m=-\infty}^{\infty}e^{im\phi_p}\left\langle E_m^p(\lambda\rho_p)d_m^p+F_m^p(\lambda\rho_p)c_m^p +\sum_{\substack{k=0\\k\neq p}}^{H}\left[\sum_{n=-M}^{M}E_{mn}^k(\lambda\rho_p)b_n^k+\sum_{n=-\infty}^{\infty}F_{mn}^k(\lambda\rho_p)a_n^k\right]\right\rangle \tag{38}$$

where

$$E_m^p(\lambda\rho_p)=\frac{\pi R_p}{4\lambda^2}\left\{J_m(\lambda\rho_p)[\alpha_m^Y(\lambda R_p)-i\alpha_m^J(\lambda R_p)]+\frac{2}{\pi}I_m(\lambda\rho_p)\alpha_m^K(\lambda R_p)\right\} \tag{39}$$

$$F_m^p(\lambda\rho_p)=-\frac{\pi R_p}{4\lambda^2}\left\{J_m(\lambda\rho_p)[\beta_m^Y(\lambda R_p)-i\beta_m^J(\lambda R_p)]+\frac{2}{\pi}I_m(\lambda\rho_p)\beta_m^K(\lambda R_p)\right\} \tag{40}$$

$$E_{mn}^k(\lambda\rho_p)=\begin{cases}\dfrac{\pi R_k}{4\lambda^2 D}e^{i(n-m)\theta_{kp}}\left\{J_{n-m}(\lambda r_{kp})J_m(\lambda\rho_p)[Y_n(\lambda R_k)-iJ_n(\lambda R_k)]\right.\\ \left.+\dfrac{2}{\pi}I_{n-m}(\lambda r_{kp})I_m(\lambda\rho_p)K_n(\lambda R_k)\right\}, & k=0\\ \dfrac{\pi R_k}{4\lambda^2}e^{i(n-m)\theta_{kp}}\left\{J_m(\lambda\rho_p)\alpha_n^J(\lambda R_k)[Y_{n-m}(\lambda r_{kp})-iJ_{n-m}(\lambda r_{kp})]\right.\\ \left.+\dfrac{2}{\pi}(-1)^m I_m(\lambda\rho_p)\alpha_n^J(\lambda R_k)K_{n-m}(\lambda r_{kp})\right\}, & k\neq 0,\ p\end{cases} \tag{41}$$

$$F_{mn}^k(\lambda\rho_p)=\begin{cases}-\dfrac{\pi R_k}{4\lambda D}e^{i(n-m)\theta_{kp}}\left\{J_{n-m}(\lambda r_{kp})J_m(\lambda\rho_p)[Y'_n(\lambda R_k)-iJ'_n(\lambda R_k)]\right.\\ \left.+\dfrac{2}{\pi}I_{n-m}(\lambda r_{kp})I_m(\lambda\rho_p)K'_n(\lambda R_k)\right\}, & k=0\\ -\dfrac{\pi R_k}{4\lambda^2}e^{i(n-m)\theta_{kp}}\left\{J_m(\lambda\rho_p)\beta_n^J(\lambda R_k)[Y_{n-m}(\lambda r_{kp})-iJ_{n-m}(\lambda r_{kp})]\right.\\ \left.+\dfrac{2}{\pi}(-1)^m I_m(\lambda\rho_p)\beta_n^I(\lambda R_k)K_{n-m}(\lambda r_{kp})\right\}, & k\neq 0,\ p\end{cases} \tag{42}$$

By differentiating Eq. (38) with respect to ρ_p, the equation of the slope θ near the circular boundary B_p is given as

$$0=\sum_{m=-\infty}^{\infty}e^{im\phi_p}\left\langle G_m^p(\lambda\rho_p)d_m^p+H_m^p(\lambda\rho_p)c_m^p +\sum_{\substack{k=0\\k\neq p}}^{H}\left[\sum_{n=-M}^{M}G_{mn}^k(\lambda\rho_p)b_n^k+\sum_{n=-\infty}^{\infty}H_{mn}^k(\lambda\rho_p)a_n^k\right]\right\rangle \tag{43}$$

where $G_m^p(\lambda\rho_p)$, $H_m^p(\lambda\rho_p)$, $G_{mn}^k(\lambda\rho_p)$ and $H_{mn}^k(\lambda\rho_p)$ are obtained by differentiating $E_m^p(\lambda\rho_p)$, $F_m^p(\lambda\rho_p)$, $E_{mn}^k(\lambda\rho_p)$ and $F_{mn}^k(\lambda\rho_p)$ in Eqs. (39)–(42) with respect to ρ_p.

By setting ρ_p to R_p and applying the orthogonal property of $\{e^{im\phi_p}\}$ ($p=0,1,\ldots,H$), Eqs. (31), (36), (38) and (43) yield

$$\begin{cases}A_m^0(\lambda R_0)d_m^0+B_m^0(\lambda R_0)c_m^0 +\sum_{k=1}^{H}\left[\sum_{n=-\infty}^{\infty}A_{mn}^k(\lambda R_0)b_n^k+\sum_{n=-\infty}^{\infty}B_{mn}^k(\lambda R_0)a_n^k\right]=0\\ C_m^0(\lambda R_0)d_m^0+D_m^0(\lambda R_0)c_m^0 +\sum_{k=1}^{H}\left[\sum_{n=-\infty}^{\infty}C_{mn}^k(\lambda R_0)b_n^k+\sum_{n=-\infty}^{\infty}D_{mn}^k(\lambda R_0)a_n^k\right]=0\\ E_m^p(\lambda R_p)d_m^p+F_m^p(\lambda R_p)c_m^p +\sum_{\substack{k=0\\k\neq p}}^{H}\left[\sum_{n=-M}^{M}E_{mn}^k(\lambda R_p)b_n^k+\sum_{n=-\infty}^{\infty}F_{mn}^k(\lambda R_p)a_n^k\right]=0\\ G_m^p(\lambda R_p)d_m^p+H_m^p(\lambda R_p)c_m^p +\sum_{\substack{k=0\\k\neq p}}^{H}\left[\sum_{n=-M}^{M}G_{mn}^k(\lambda R_p)b_n^k+\sum_{n=-\infty}^{\infty}H_{mn}^k(\lambda R_p)a_n^k\right]=0\end{cases}, \tag{44}$$

for $m=0,\ \pm1,\ \pm2,\ldots$; $n=0,\ \pm1,\ \pm2,\ldots$; $p=1,\ldots,H$.

Eq. (44) is a coupled infinite system of simultaneous linear algebraic equations which is an analytical model for the free vibration of a circular plate with multiple circular holes. These coefficients a_m^k, b_m^k, c_m^k and d_m^k ($k=0,\ldots,H$) are determined by the boundary conditions. In the following computation, only the finite M terms are used in Eq. (44). According to the direct-searching scheme [12], the natural frequencies are determined by

finding the drop of the minimum singular value of the influence matrix of the truncated finite system from Eq. (44) by performing the frequency sweep. Once the eigenvalues are found, the associated mode shapes can be obtained by substituting the corresponding boundary eigenvectors (i.e. the complex Fourier series for the boundary density) into the boundary integral equations.

4. Spurious eigenvalues for multiply-connected plate eigenproblems using the BEM

For the 2-D multiply-connected problem [17], spurious eigenvalues occur when using the BEM even though the complex-valued kernel function is employed to solve the eigenproblem. This may mislead the wrong judge of true eigenvalues. Consequently, the SVD updating technique is adopted to suppress the appearance of spurious eigenvalue. The concept of this technique is to provide sufficient constrains to overcome the rank deficiency of the system.

The approach to suppress the appearance of spurious frequency is the criterion of satisfying Eqs. (12)–(15) at the same time.

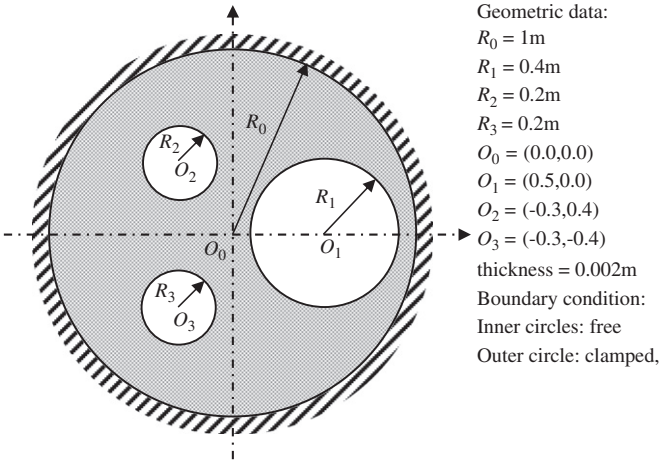

Fig. 4. A circular clamped plate with three circular free holes.

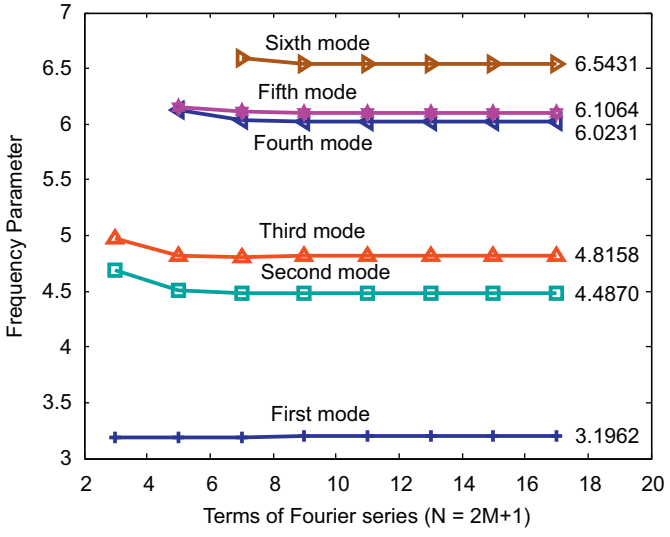

Fig. 5. Natural frequency parameter versus the number of terms of Fourier series for a circular clamped plate with three circular free holes.

In Section 3, the first and the second null field equations (i.e. Eqs. (12) and (13)) are employed in the formulation which is called the *UΘ* formulation. To provide sufficient constrains, the *UM* formulation is an alternative. Applying the moment operator of Eq. (23) to Eq. (31) with respect to the field point ρ_0 and to Eq. (38) with respect to the field point ρ_p we have, respectively,

$$0=\sum_{m=-\infty}^{\infty} e^{im\phi_0}\left\langle P_m^0(\lambda\rho_0)d_m^0+Q_m^0(\lambda\rho_0)c_m^0 + \sum_{k=1}^{H}\left[\sum_{n=-\infty}^{\infty}P_{mn}^k(\lambda\rho_0)b_n^k+\sum_{n=-\infty}^{\infty}Q_{mn}^k(\lambda\rho_0)a_n^k\right]\right\rangle, \tag{45}$$

$$0=\sum_{m=-\infty}^{\infty} e^{im\phi_p}\left\langle S_m^p(\lambda\rho_p)d_m^p+T_m^p(\lambda\rho_p)c_m^p + \sum_{\substack{k=0\\k\neq p}}^{H}\left[\sum_{n=-M}^{M}S_{mn}^k(\lambda\rho_p)b_n^k+\sum_{n=-\infty}^{\infty}T_{mn}^k(\lambda\rho_p)a_n^k\right]\right\rangle, \tag{46}$$

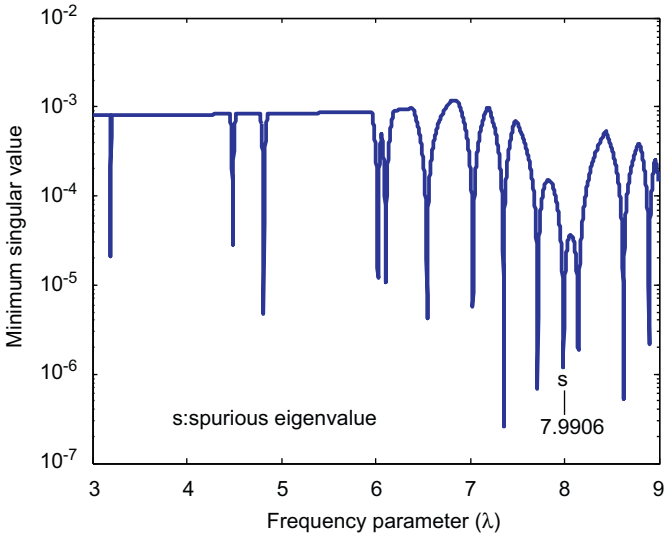

Fig. 6. The minimum singular value versus the frequency parameter by using the *UΘ* formulation for a circular clamped plate with three circular free holes.

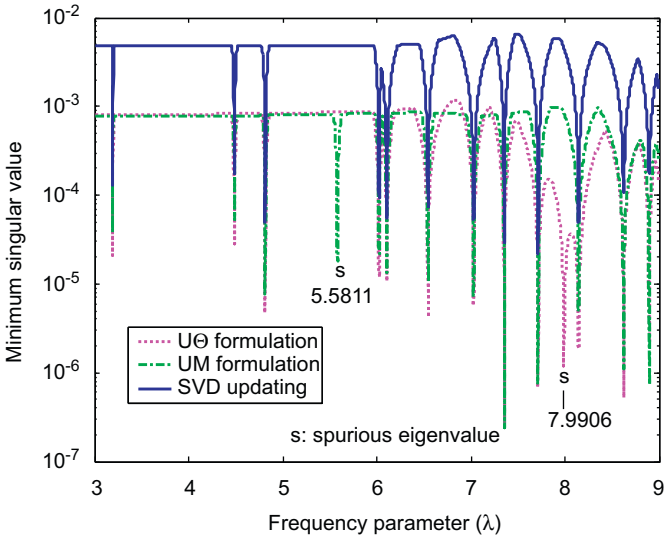

Fig. 7. The minimum singular value versus the frequency parameter by using the *UΘ* formulation, *UM* formulation and SVD updating technique for a circular clamped plate with three circular holes.

where $P_m^0(k\rho_0)$, $Q_m^0(k\rho_0)$, $P_{mn}^k(k\rho_0)$ and $Q_{mn}^k(k\rho_0)$, can be obtained by applying the moment operator to $A_m^0(k\rho_0)$, $B_m^0(k\rho_0)$, $A_{mn}^k(k\rho_0)$ and $B_{mn}^k(k\rho_0)$ with respect to ρ_0; $S_m^p(\lambda\rho_p)$, $T_m^p(\lambda\rho_p)$, $S_{mn}^k(\lambda\rho_p)$ and $T_{mn}^k(\lambda\rho_p)$ can be determined similarly from $E_m^p(\lambda\rho_p)$, $F_m^p(\lambda\rho_p)$, $E_{mn}^k(\lambda\rho_p)$ and $F_{mn}^k(\lambda\rho_p)$ with respect to ρ_p.

By setting ρ_p to R_p and applying the orthogonal property of $\{e^{im\phi_p}\}$ ($p=0, 1,\ldots,H$), Eqs.(31), (45), (38) and (46) yield

$$\begin{cases} A_m^0(\lambda R_0)d_m^0 + B_m^0(\lambda R_0)c_m^0 \\ \quad + \sum_{k=1}^{H}\left[\sum_{n=-\infty}^{\infty} A_{mn}^k(\lambda R_0)b_n^k + \sum_{n=-\infty}^{\infty} B_{mn}^k(\lambda R_0)a_n^k\right] = 0 \\ P_m^0(\lambda R_0)d_m^0 + Q_m^0(\lambda R_0)c_m^0 \\ \quad + \sum_{k=1}^{H}\left[\sum_{n=-\infty}^{\infty} P_{mn}^k(\lambda R_0)b_n^k + \sum_{n=-\infty}^{\infty} Q_{mn}^k(\lambda R_0)a_n^k\right] = 0 \\ E_m^p(\lambda R_p)d_m^p + F_m^p(\lambda R_p)c_m^p \\ \quad + \sum_{\substack{k=0 \\ k\neq p}}^{H}\left[\sum_{n=-M}^{M} E_{mn}^k(\lambda R_p)b_n^k + \sum_{n=-\infty}^{\infty} F_{mn}^k(\lambda R_p)a_n^k\right] = 0 \\ S_m^p(\lambda R_p)d_m^p + T_m^p(\lambda R_p)c_m^p \\ \quad + \sum_{\substack{k=0 \\ k\neq p}}^{H}\left[\sum_{n=-M}^{M} S_{mn}^k(\lambda R_p)b_n^k + \sum_{n=-\infty}^{\infty} T_{mn}^k(\lambda R_p)a_n^k\right] = 0 \end{cases}, \quad (47)$$

for $m=0, \pm1, \pm2,\ldots$; $n=0, \pm1, \pm2,\ldots$; $p=1,\ldots,H$, which is called the *UM* formulation.

To obtain an overdetermined system, we can combine Eqs. (44) and (47) by using the SVD technique of updating terms. In other words, natural frequencies without spurious ones can be obtained by using the SVD technique to the complete system which includes Eqs. (44) and (47).

5. Numerical results and discussions

To demonstrate the validity of proposed method, the FORTRAN code was implemented to determine natural frequencies and modes of a circular plate with multiple circular holes. It was independently solved by using the FEM (the ABAQUS software) for comparison. The inner boundary is subject to the free boundary condition. The thickness of plate is 0.002 m and the Poisson's ratio is $\mu=1/3$. The general-purpose linear triangular elements of type S3 were employed to model the flexural plate problem by using the ABAQUS. Although the thickness of the flexural plate is 0.002 m, these elements do not suffer from the transverse shear locking based on the theoretical manual of ABAQUS [14].

A circular plate with three holes is considered as shown in Fig. 4. The radii of holes are 0.4, 0.2 and 0.2 m and the coordinates of the centers are (0.5,0), (−0.3,0.4) and (−0.3,−0.4), respectively, in the coordinate system with the origin at the center of outer circle. The lower six natural frequency parameters versus the numbers of terms of Fourier series N are shown in Fig. 5. It can be seen that the proposed solution promptly converges with few terms of Fourier series. By using the *UΘ* formulation and thirteen terms of Fourier series ($N=13$), the minimum singular value of the influence matrix versus the frequency parameter λ is shown in Fig. 6. Since the direct-searching scheme is used, the drop location indicates the possible eigenvalue. The spurious eigenvalue of 7.9906 occurs when using the *UΘ* formulation and it is found to be the true eigenvalue of a clamped circular plate with a radius of 0.4 m. Fig. 7 shows the minimum singular value of the influence matrix versus the frequency parameter λ by using three different approaches: the *UΘ* formulation (dotted line), the *UM* formulation (dot–dashed line) and the SVD updating technique (solid line). It indicated that the spurious eigenvalue of 5.5811 occurs when using the *UM* formulation and it is the true eigenvalue of a simply

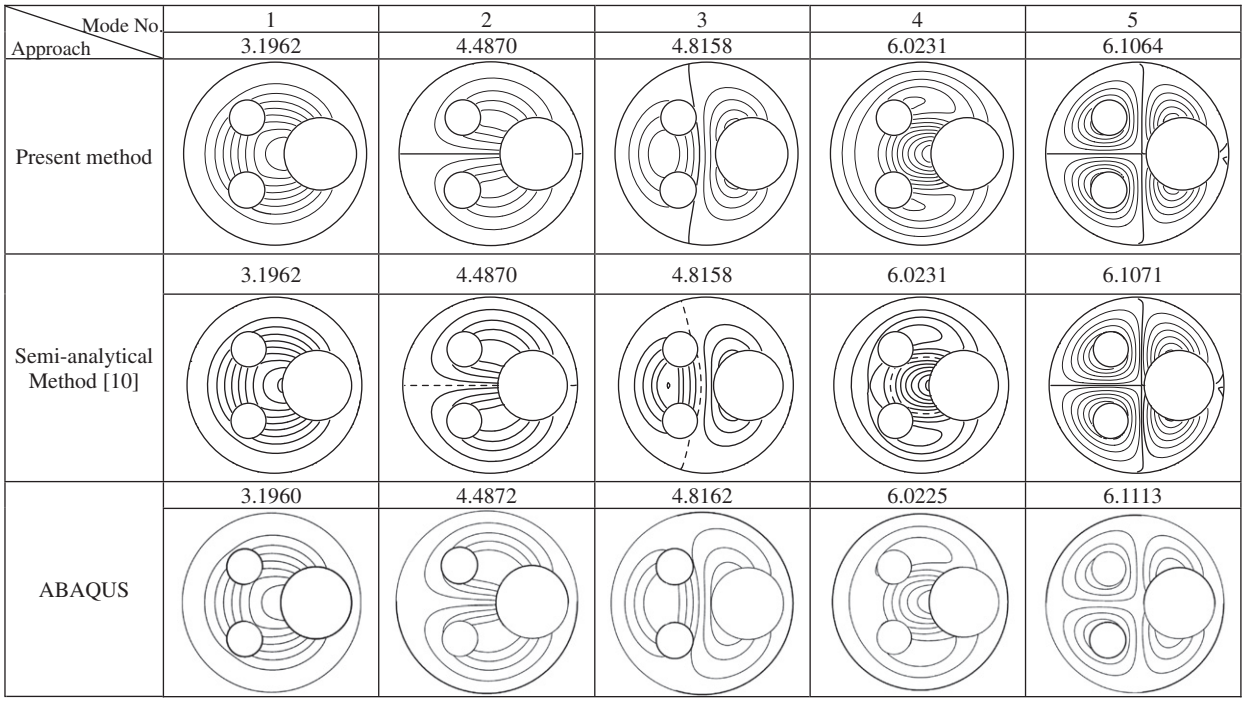

Fig. 8. The lower five natural frequency parameters and mode shapes for a circular clamped plate with three circular free holes by using the present method, the semi-analytical method and the FEM.

supported circular plate with a radius of 0.4 m. It demonstrates that the spurious eigenvalue can be filtered out by using the SVD updating technique. The same problem is also solved by using the ABAQUS and its model needs 308 960 elements in order to obtain acceptable results for comparison. The lower five natural frequency parameters and modes by using the present method, the semi-analytical method [10] and the FEM are shown in Fig. 8. Good agreement between the results of the present method and those of the ABAQUS is observed.

6. Concluding remarks

The free vibration analysis of a circular plate with multiple circular holes has been done in an analytical way. The proposed method consists of the null field integral formulation, the addition theorem and complex Fourier series. Owing to the addition theorem, two critical issues for the improper integration in the boundary integration equation and the higher order derivatives in the multiply-connected domain problems were successively solved in a novel way. By satisfying the boundary conditions, a coupled infinite system of simultaneous linear algebraic equations was derived with no approximation. By truncating the higher order terms, natural frequencies and modes were numerically determined by using the SVD technique. The convergence analysis was examined on the number of terms for the complex Fourier series. A numerical example for a clamped circular plate with three circular holes was presented. The proposed results match well with those provided by the FEM where a huge number of elements were required to obtain acceptable solutions for comparison. Numerical results show that the SVD technique of updating terms can successfully suppress the appearance of spurious eigenvalues.

Acknowledgements

Financial support from the National Science Council under the Grant No. NSC-98-2221-E-157 and NSC-97-2221-E-019-015-MY3 for China University of Science and Technology and Taiwan Ocean University, repectively, is gratefully acknowledged.

References

[1] Khurasia HB, Rawtani S. Vibration analysis of circular plates with eccentric hole. ASME Journal of Applied Mechanics 1978;45:215–7.
[2] Leissa AW, Narita Y. Natural frequencies of simply supported circular plates. Journal of Sound and Vibration 1980;70:221–9.
[3] Vogel SM, Skinner DW. Natural frequencies of transversely vibrating uniform annular plates. ASME Journal of Applied Mechanics 1965;32:926–31.
[4] Vega DA, Vera SA, Sanchez MD, Laura PAA. Transverse vibrations of circular, annular plates with a free inner boundary. Journal of the Acoustical Society of America 1998;103:1225–6.
[5] Vera SA, Sanchez MD, Laura PAA, Vega DA. Transverse vibrations of circular, annular plates with several combinations of boundary conditions. Journal of Sound and Vibration 1998;213(4):757–62.
[6] Vera SA, Laura PAA, Vega DA. Transverse vibrations of a free-free circular annular plate. Journal of Sound and Vibration 1999;224(2):379–83.
[7] Cheng L, Li YY, Yam LH. Vibration analysis of annular-like plates. Journal of Sound and Vibration 2003;262:1153–70.
[8] Laura PAA, Masia U, Avalos DR. Small amplitude, transverse vibrations of circular plates elastically restrained against rotation with an eccentric circular perforation with a free edge. Journal of Sound and Vibration 2006;292:1004–10.
[9] Lee WM, Chen JT. Free vibration analysis of circular plates with multiple circular holes using indirect BIEMs. Journal of Sound and Vibration 2007;304:811–30.
[10] Lee WM, Chen JT. Null-field integral equation approach for free vibration analysis of circular plates with multiple circular holes. Computational Mechanics 2008;42:733–47.
[11] Providatis CP, Beskos DE. Dynamic analysis of plates by boundary elements. ASME Applied Mechanics Reviews 1999;52(7):213–36.
[12] Kitahara M. Boundary integral equation methods in eigenvalue problems of elastodynamics and thin plates. Amsterdam: Elsevier; 1985.
[13] IMSL Math/Library Volumes 1 and 2 version 4.01 Visual Numerics, Inc., 1999.
[14] ABAQUS/CAE 6.5 Hibbitt, Karlsson and Sorensen, Inc., RI, 2004.
[15] Watson GN. A treatise on the theory of Bessel functions. 2nd ed. Cambridge: Cambridge Library edition; 1995.
[16] Gradshteyn IS, Ryzhik IM. Table of integrals, series, and products. 5th ed. New York: Academic Press; 1996.
[17] Chen JT, Liu LW, Hong HK. Spurious and true eigensolutions of Helmholtz BIEs and BEMs for a multiply-connected problem. Proceedings of the Royal Society of London Series A 2003;459:1891–924.